Journal of Power Sources 183 (2008) 76–83

Contents lists available at ScienceDirect

Journal of Power Sources

journal homepage: www.elsevier.com/locate/jpowsour

Synthesis and characterization of new ternary transition metal sulfide anodes for H_2S-powered solid oxide fuel cell

V. Vorontsov, J.L. Luo*, A.R. Sanger, K.T. Chuang

Department of Chemical and Materials Engineering, University of Alberta, Edmonton, Alberta T6G 2G6, Canada

ARTICLE INFO

Article history:
Received 23 March 2008
Received in revised form 23 April 2008
Accepted 23 April 2008
Available online 2 May 2008

Keywords:
H_2S
SOFC
Ternary transition metal sulfides
Polarization resistance
Molybdenum sulfide
Vanadium sulfide

ABSTRACT

A number of ternary transition metal sulfides with general composition AB_2S_4 (where A and B are different transition metal atoms) have been prepared and investigated as potential anode catalysts for use in H_2S-powered solid oxide fuel cells (SOFCs). For the initial screening, polarization resistance of the materials was measured in a two electrode symmetrical cell at 700–850 °C. Vanadium-based materials showed the lowest polarization resistance, and so were chosen for subsequent full cell tests using the configuration [H_2S, AV_2S_4/YSZ/Pt, air] (where A = Ni, Cr, Mo). MoV_2S_4 anode had superior activity and performance in the full cell setup, consistent with results from symmetrical cell tests. Polarization curves showed MoV_2S_4 had the lowest potential drop, with up to a 200 mA cm^{-2} current density at 800 °C. The highest power density of ca. 275 mW cm^{-2} at 800 °C was obtained with a pure H_2S stream. Polarization resistance of materials was a strong function of current density, and showed a sharp change of slope attributable to a change in the rate-limiting step of the anode reaction mechanism. MoV_2S_4 was chemically stable during prolonged (10 days) exposure to H_2S at 850 °C, and fuel cell performance was stable during continuous 3-day operation at 370 mA cm^{-2} current density.

1. Introduction

Currently over 40×10^6 tons of hydrogen sulfide are generated world-wide as by-product from the petroleum, natural gas and coal gasification industries [1]. Its concentration ranges from a few ppm to above 80% in refining and natural gas industries. The adverse effects of H_2S on industrial processes, human health and the environment make it necessary to remove it from all effluent streams. There are few direct commercial uses for H_2S; hence most of it is converted to sulfur in the two-step Claus process. The overall reaction is highly exothermic and although some of the heat can be recovered as steam it would be far more desirable to either directly recover hydrogen or to electrochemically oxidize H_2S in situ at the anode of a solid oxide fuel cell (SOFC). Hydrogen is a high commodity valuable product and fuel cells would allow direct conversion of the overall Claus reaction free energy change into direct current (DC) electricity with efficiency as high as 80% for an integrated system.

The approaches for hydrogen production from H_2S including electrolytic, photochemical, thermal and thermo-catalytic dissociation of H_2S followed by selective product separation utilizing membrane reactors or thermal diffusion columns to increase hydrogen production have been comprehensively reviewed by Zaman and Chakma [2]. None of these previous approaches have gained commercial success due to either high-energy input requirements to drive the dissociation reaction or insufficient production efficiency.

One of the major technical challenges in the development of H_2S/O_2 SOFC is to identify anode materials that are conductive, chemically and electrochemically stable, and catalytically active in H_2S-rich environments. In the last 20 years many groups have investigated several materials as potential candidates as anodes for SOFC operated on H_2S [3–8]. Unfortunately, none of these materials fully satisfies criteria required for a successful and effective anode. In particular, two main technological requirements have to be fulfilled for commercial applications of SOFC anodes: low polarization resistance and long-term stability.

Our group has previously investigated performance of $Ni_{3\pm x}S_2$, CoS, FeS, MoS_2 and their combinations as anode materials in the temperature range 700–850 °C [9,10]. MoS_2 admixed 1:1 by weight with $Ni_{3\pm x}S_2$ showed the highest activity with maximum power density of 45 mW cm^{-2} at 800 °C in [H_2S, $Ni_{3\pm x}S_2$–MoS_2/YSZ (0.3-mm thick)/Pt, air] fuel cell configuration. We have also developed proprietary formulations with superior performance by mechanical mixing these composite sulfides with Ag and YSZ powders to improve conductivity and electrochemical reaction volume, respec-

* Corresponding author. Tel.: +1 780 492 2232; fax: +1 780 492 2881.
E-mail address: jingli.luo@ualberta.ca (J.L. Luo).

0378-7753/$ – see front matter © 2008 Elsevier B.V. All rights reserved.
doi:10.1016/j.jpowsour.2008.04.055

tively [11]. A power density of 70 mW cm^{-2} was achieved at 800 °C in [H_2S, $Ni_{3\pm x}S_2$–MoS_2–Ag–YSZ/YSZ (0.3-mm thick)/Pt, air] fuel cell configuration. Although this type of anode has shown excellent kinetic behavior, our further detailed investigation of MoS_2 and $Ni_{3\pm x}S_2$ composite anode showed its insufficient long-term stability [12]. Herein we report superior performance of new ternary metal sulfides with general composition AB_2S_4 (where A was selected from Mo, Cr, Ni, Fe, Co, and Cu, and B was selected from V, Cr, and Mo) [13].

The goal of this work was to measure the polarization resistance and fuel cell performance of both known and newly developed composite sulfide anode materials and verify their chemical and electrochemical stability in H_2S atmosphere at 700–850 °C.

2. Experimental

2.1. Preparation of anode materials

Because of the problems encountered in using metallic materials and simple sulfides, our group initiated an investigation into potential anodes for H_2S-powered SOFC, the anodes comprising several ternary metal sulfides with general composition AB_2S_4 (where A was selected from Mo, Cr, Ni, Fe, Co, and Cu, and B was selected from V, Cr, and Mo) known for their high thermal and chemical stability in H_2S-rich atmospheres [13]. The anodes used herein are from those studies.

All thiospinel materials were prepared by mixing appropriate quantities of finely dispersed powdered elements (purity > 99.9%; all from Alfa Aesar) and grinding in *iso*-propanol for preparation of well mixed dispersions, then drying, followed by their placement into a quartz ampule. After evacuation and ampule sealing, the reaction mixture was slowly heated (1 °C min^{-1}) to 900 °C and kept at this temperature for 48 h, during which time solid-state reaction occurred. The procedure was repeated twice with one intermediate re-grinding to obtain good sample homogeneity. The resulting reaction product was ground with 40 wt% YSZ powder (Tosoh, Japan) in *iso*-propanol in preparation for use as an anode electrocatalyst. For comparison, composite sulfide catalysts Mo–Ni–S were prepared following the same procedure as in [12] followed by addition of 5 wt% of both YSZ and Ag (<325 mesh, Alfa Aesar) to increase the electrochemical reaction zone and facilitate transport of charge within the anode volume, as described in Ref. [11].

2.2. Electrolyte and cathode

Yttria-stabilized–zirconia (8 mol% YSZ) is a favored electrolyte material due to its relatively high ionic conductivity and proven stability in H_2S atmospheres. In this work Pt was used as the cathode; it is recognized that alternative cathode catalysts will also be effective.

2.3. Cell preparation

Anode catalyst powders initially mixed with α-terpineol to make a paste were applied onto 0.3-mm thick YSZ disks (Intertec Southwest ZO-8Y, 25.4 mm diameter). To enhance the adhesion between the electrode and the YSZ disk, the surfaces of the electrolyte first were manually roughened by mechanical grinding using silicon carbide powder, and then cleaned. Symmetrical one-atmosphere cells had the general configuration [electrode/YSZ/electrode]. Pt paste (Heraeus) was painted on the opposite side of the electrolyte from the anode to prepare the asymmetric cell configuration [anode/YSZ/Pt]. In three electrode cells, a Pt reference electrode was applied on the same side of YSZ electrolyte as the cathode. After drying for several hours under an IR lamp at room temperature, disks were fired at 1050 °C for 2 h in N_2 flow to achieve good adhesion of electrodes to the membrane. In all cases anodes had a geometrical area ca. 1 cm^2 and were ca. 30–50 μm thick.

2.4. Experimental setup

Details of installation of the membrane electrode assembly (MEA) can be found in Ref. [10]. In brief, the MEA was securely bonded between two co-axial pairs of cylindrical alumina tubes. The inner tubes served as the respective anode and cathode feed lines and outer ones as exhaust. The perimeter of each outer cylinder was sealed to the membrane electrode assembly by applying a thin layer of ceramic adhesive (Aremco 503). The whole operating section of the assembly was placed in a Thermolyne F79300 tubular furnace, while the ends of the alumina tubes extended outside the furnace to allow connections of feed and exhaust gases. The cell was heated to an operating temperature under a stream of high purity (99.999%) N_2.

Au wires with spot-welded mesh (0.5 mm 99.5% Alfa Aesar) were used as current collectors in the symmetrical set-up. In the asymmetric cell, Pt wires with spot-welded mesh (0.5 mm 99.5% Alfa Aesar) were used as cathode and reference electrode current collectors, while Au served as anode current collector. Perforated plates made from Macor machinable ceramic were used on both sides of the membrane assembly to provide support and to ensure good contact of current collectors with electrodes.

2.5. Electrochemical characterization

All experiments were conducted in the temperature range 700–850 °C. After the temperature was stable, flow rates of H_2S 25 cm^3 min^{-1} and air 50 cm^3 min^{-1} (both gases from Praxair) were introduced to anode and cathode sides of the MEA in full cell tests. For symmetrical cell measurements, the anode feed flow was saturated with water vapor by passing anode feed through a water bath at room temperature. All electrochemical testing was done using Solartron 1255B frequency response analyzer connected with Solartron electrochemical interface SI 1287 system. Impedance measurements were performed in the frequency range 100 kHz to 0.01 Hz under open circuit voltage (OCV) using 10 mA AC voltage. Potentiodynamic curves were recorded at a scanning rate of 1 mV s^{-1}. Data were analyzed using ZView and CorrView software packages from Scribner Associates.

2.6. Anode material characterization

Phase composition and chemical stability of fresh and after-test samples were analyzed using X-ray diffraction (XRD) with a Rigaku Rotaflex X-ray diffractometer employing a Co anode. After each test, the samples were visually inspected to determine the occurrence and extent of delamination of electrode materials from YSZ disks. Images and composition of fresh and used anodes were obtained using scanning electron microscopy with X-ray energy dispersive analysis (SEM–EDX) using a Hitachi S-2700 scanning electron microscope equipped with a PGT IMIX digital imaging system and a PGT PRISM IG detector for EDX.

3. Results and discussion

3.1. Phase analysis by XRD

Ternary chalcogenides of the type AB_2X_4 (A and B = transition metals and X = S, Se, Te) generally adopt either the cubic spinel

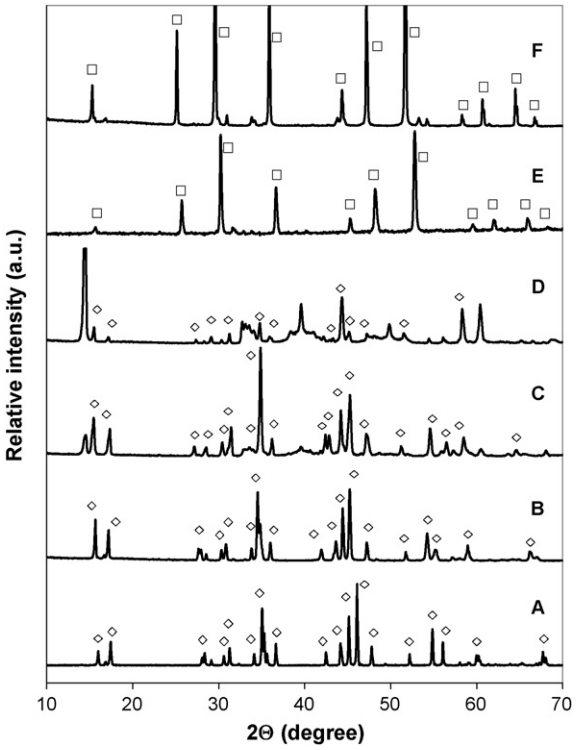

Fig. 1. XRD spectra of (A) NiV_2S_4; (B) CrV_2S_4; (C) MoV_2S_4; (D) $CoMo_2S_4$; (E) $CuCr_2S_4$; (F) $FeCr_2S_4$. Crystal structures: (◊) monoclinic; (□) cubic.

structure or defect structures related to NiAs. Both the metal ions and polarizability of the anions determine which of these structures is favored. In the cubic close-packed anion array of the thiospinel lattice the metal ions occupy both octahedral and tetrahedral interstices. However, in a nearly hexagonal close-packed array of the NiAs structure, the metal ions occupy only octahedral interstices. The defect structures related to NiAs can further be classified into three types, of which monoclinic defect NiAs or Cr_3S_4-type structures are most common. The structure type and distance between A and B cations have strong effects on chemical and electrical properties of transition metal sulfides [14].

Fig. 1 presents XRD patterns for all materials synthesized in this work. A match was found between XRD of our NiV_2S_4 sample and PDF 00-036-1132 of NiV_2S_4. Another phase also was present in small amount, but we were not able to identify it. XRD peaks in PDF 01-074-1294 of MoV_2S_4 were the predominant matches with those for our sample of MoV_2S_4, and trace amounts of MoS_2-2H with PDF 65-7025 also were present. A $CoMo_2S_4$ sample contained $CoMo_2S_4$, PDF 00-023-0192, a lesser but substantial amount of MoS_2-2H (hexagonal), PDF 65-7025, and a trace of MoS_2-3R (rhombohedral), PDF 77-0341. XRD of a CrV_2S_4 sample comprised only peaks for $Cr_{0.99}V_{1.8}S_4$ single phase PDF 01-089-5597. Although a higher stoichiometric amount of vanadium was expected based on the composition of the reaction mixture, we did not detect any other phase.

After $CuCr_2S_4$ synthesis some elemental sulfur was condensed on the walls of the quartz ampule. It is possible that some transient CuS phase was formed during the solid-state reaction, although it is only thermodynamically stable at temperatures below 550 °C. When heated to higher temperatures, CuS decomposes into Cu_2S and S phases. The sample was heated again and held at 550 °C for 3 days. XRD results showed the existence of only cubic $CuCr_2S_4$ single phase, PDF 03-065-4606. The XRD of our $FeCr_2S_4$ sample showed that it was predominantly $FeCr_2S_4$ phase, PDF 01-089-2617, along with a small amount of Fe_7S_8, PDF 01-089-1954. Thus, although the synthesis method chosen in this work was not optimized with respect to obtaining desired single-phase materials, the products were fully reproducible and characterizable materials of sufficient purity to enable initial screening as anode catalysts.

3.2. Material selection—symmetrical cell

For the symmetrical cells, the measured electrode response represents the sum of the two nominally identical electrodes. In the figures the electrode response is divided by two. This means that the polarization resistance from the plots is the average of values from the two electrodes. From impedance spectra the overall electrode polarization resistance for H_2S oxidation (R_p) was obtained from the difference of the intercepts of the electrode arcs on the real impedance axis at low ($f \rightarrow 0$ Hz) and high frequencies ($f \cong 10^5$ Hz). Ohmic resistance of the entire cell R_s was obtained as the high frequency intercept of the impedance with the real axis.

The commonly observed impedance spectrum of solid electrolyte/electrode systems is rarely in the form of semicircular arcs and instead consists typically of depressed arcs. The arcs can often be skewed to the low or the high end of the frequency spectrum. This type of behavior often indicates heterogeneity in the system and distribution of time constants, and can be simulated by including distributed or constant-phase elements (CPEs) in the equivalent circuit. Obtained impedance spectra were fitted using non-linear-least-squares algorithm utilized in Zview, from Scribner Associates, normally using the following equivalent circuit: $LR_s(R_pQ)_i$. No strict physical meaning was given a priori to any circuit elements. In the above equivalent circuit L is an inductance, primary ascribed to the measuring leads, R_s is ohmic resistance of the entire cell, Q is constant phase element with admittance $Y = Y_0(j\omega)^n$ and i represents a number of (R_pQ) sub-elements in series. Acceptable agreement was observed between model curves and experimental data, and the error $[(Z_{measured} - Z_{fit})/Z_{measured}]$ for all cell results was less than 2% [15].

Depending on the material and cell temperature, recorded impedance spectra contained one to three distinct arcs (depressed semicircles), each representative of different types of electrochemical and/or physical–chemical transport processes. The focus of the present study was on comparison of polarization resistance of all anode materials under identical experimental conditions, and so does not at this time include a detailed investigation of individual components of electrochemical impedance spectroscopy (EIS) spectra. Table 1 summarizes the results for measurements of symmetrical cells. Summit frequencies f_s were calculated using the following equation:

$$f_s = \frac{1}{2\pi \sqrt[n]{RY_0}} \quad (1)$$

Table 1
Polarization resistances of materials under investigation broken down into individual components of EIS spectra by frequency domain[a]

Anode materials	R_p^{HF} (Ω cm^2) ($f_{summit} > 1$ kHz)	R_p^{MF} (Ω cm^2) ($f_{summit} \cong 200$ Hz)	R_p^{LF} (Ω cm^2) ($f_{summit} < 1$ Hz)
Mo–Ni–S	13.2	15.3	0.9
$CoMo_2S_4$	35.0	–	1.2
$FeCr_2S_4$	60.0	–	1.9
$CuCr_2S_4$	12.6	–	3.0
CrV_2S_4	2.8	–	1.2
NiV_2S_4	0.4	–	2.1
MoV_2S_4	0.2	–	1.3

[a] Cell configuration: [electrode/YSZ/electrode] using 97% H_2S–3% H_2O gas feed at 800 °C. Values for HF, MF and LF are f_{summit} for high, medium and low frequency arcs.

There exists a small level of uncertainty in the calculated values for summit frequencies of each process, as there may be further small arcs present that are not readily resolved from their overlap with other, larger arcs.

Details of EIS measurements will now be presented individually for materials synthesized, and their suitability for electrochemical cell applications will be evaluated.

3.2.1. $FeCr_2S_4$

Two dominant arcs were observed with characteristic frequencies 1–4 kHz for the high frequency (HF) contribution and 0.3–0.1 Hz for the low frequency (LF) component, and polarization resistances of 60.1 Ω cm^2 and 1.9 Ω cm^2 for HF and LF components, respectively. The HF component showed a temperature-activated behavior with an activation energy (E_a) of 0.92 eV while the LF component was not temperature dependent ($E_a^{LF} \cong 0$). After 20 h in a stream of H_2S at 850 °C the HF polarization resistance R_p^{HF} decreased by 25% while the value of R_p^{LF} was essentially unchanged. In all of the experiments performed using this anode material, its ohmic resistance was quite high which, together with high polarization resistance, make it an unsuitable candidate for SOFC running on H_2S fuel.

3.2.2. $CoMo_2S_4$

Cobalt and molybdenum sulfide catalysts show excellent performance for both thermocatalytic decomposition of H_2S and hydrodesulfurization process in the range 400–800 °C. Therefore it was of interest to test Co–Mo thiospinel as a potential anode catalyst for a H_2S fuel cell oxidation reaction. In the impedance spectra for $CoMo_2S_4$ anode at 800 °C two processes dominated with characteristic frequencies at 15–20 kHz (HF) and 0.1–0.2 Hz (LF). Resistances were 34.3 Ω cm^2 and 1.0 Ω cm^2 for high and low frequency arcs. Although the HF arc showed some temperature-activated behavior, a rapid increase in R_p^{HF} did not allow determination of its activation energy. This deterioration was more pronounced at higher temperatures. The LF component was unaffected by temperature change and was stable during 12 h exposure to the H_2S stream. This dynamic behavior partially could be attributed to microstructural changes of anode material with time, which were observed using SEM. The material after test was aggregated and appeared to be covered with sulfur. The initial ohmic resistance of this material was quite high and it increased with time. Thus $CoMo_2S_4$ is unlikely to be suitable as anode catalyst for H_2S-powered SOFC under the operating conditions of interest.

3.2.3. $CuCr_2S_4$

Impedance spectra for $CuCr_2S_4$ anodes showed contributions from two main processes at all temperatures within the range 750–850 °C. The characteristic frequencies were 0.7–1.5 kHz (HF) and 1.0–1.5 Hz (LF) with corresponding polarization resistances 12.6 Ω cm^2 and 3.0 Ω cm^2 at 800 °C. Polarization resistance of the HF component was temperature-activated with E_a = 0.5 eV while the LF component was essentially temperature independent. Both HF and LF components were stable during 6 h tests. Ohmic resistance R_s was 9.6 Ω cm^2 and increased with time by 4%. This high resistance (both R_p and R_s) means that $CuCr_2S_4$ has limited potential for use as an anode catalyst.

3.2.4. CrV_2S_4

Impedance spectra of CrV_2S_4 anode at 800 °C contained contributions from two dominating processes which had characteristic frequencies at 0.5–2.0 kHz (HF) and 0.2 Hz (LF). Polarization resistances were 2.8 Ω cm^2 and 1.2 Ω cm^2 for HF and LF components at 800 °C. R_p^{HF} is highly temperature-activated with activation energy 1.15–1.2 eV while R_p^{HF} is essentially unaffected by temperature. This material showed good short-term stability with no decrease in polarization resistance R_p^{HF} over 8 h exposure to H_2S at 850 °C. The material's ohmic resistance had a stable value of 0.44 Ω which indicates a highly conductive electrode. Its low resistance and high stability make CrV_2S_4 a good candidate for use as an anode catalyst for electrochemical oxidation of H_2S.

3.2.5. MoV_2S_4

EIS spectra of MoV_2S_4 anode material at 800 °C were dominated by two processes at 12–10 kHz and 0.2 Hz frequency. The polarization resistances obtained at 800 °C were 0.2 Ω cm^2 (HF) and 1.3 Ω cm^2 (LF). R_p^{HF} was temperature-activated with E_a ca. 0.52 eV. R_p^{LF} was almost unaffected or slightly activated by temperature. Overall cell polarization resistance was the lowest among all present anode materials tested. Performance was stable during 8 h exposure to H_2S stream, with less than 1% increase in R_p^{HF}. Excellent ohmic resistance was achieved (0.22 Ω at 800 °C), which showed that MoV_2S_4 has high electronic conductivity. Thus MoV_2S_4 is an excellent candidate as an anode catalyst for use in SOFC at 700–850 °C, and in particular for use with H_2S as fuel.

3.2.6. NiV_2S_4

In NiV_2S_4 spectra two major components again were observed at 10 kHz and 0.25 Hz. Polarization resistances were ca. 0.4 Ω cm^2 and 2.1 Ω cm^2 for HF and LF components, respectively. HF polarization resistance was a temperature-activated process with E_a around 0.5–0.8 eV. The value of R_p^{HF} fluctuated with time, and so it was not possible to determine a precise value for its activation energy. The LF process was stable and had an E_a ca. 0.2 eV. Ohmic resistance of NiV_2S_4 was 0.1 Ω at 800 °C and was the lowest among all of the materials tested. Hence, provided the fluctuations in value of R_p^{HF} can be limited and do not compromise its use and stability, NiV_2S_4 is a promising anode material.

3.2.7. Comparison with Ni–Mo–S composite catalysts

Our previous investigations have shown excellent performance in H_2S-powered SOFC of Ni–Mo–S composite anodes admixed with 5 wt% each of Ag and YSZ powders [11]. Consequently, it was of interest to compare its polarization resistance as an anode catalyst with the above AB_2S_4 materials. Fig. 2 presents absolute values for all anode materials under investigation compared to benchmark Ni–Mo–S composite anode at 800 °C. For Ni–Mo–S, three major contributions were observed with arcs at 10–7 kHz (HF), 200–400 Hz (MF) and 1 Hz summit frequency. This material had high polarization resistances of 13.24 Ω cm^2, 15.3 Ω cm^2 and 0.92 Ω cm^2 for

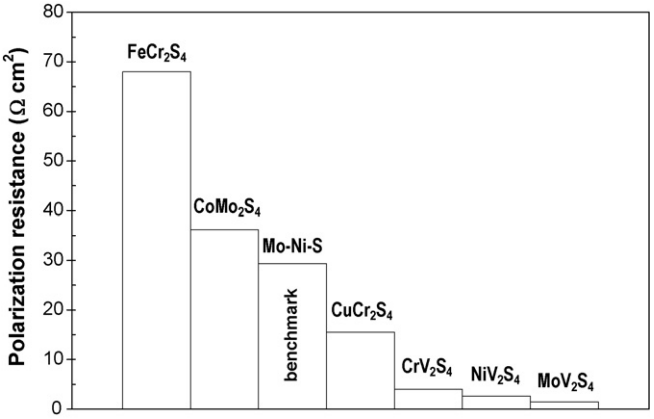

Fig. 2. Anodic polarization resistances in symmetrical cell at 800 °C.

high, medium and low frequency components. HF and MF processes were temperature-activated with activation energies of 1.26 eV and 0.52 eV. The third LF process showed no temperature dependence.

For all materials, good adhesion between anode and YSZ electrolyte was shown using optical microscopic examinations before and after the tests. Also, there were no color changes during the tests. The macroscopic structures of all materials except NiV_2S_4 were stable, and they retained their highly open porous structures after experiments, as shown in Fig. 3 for the example of vanadium-based anodes. Among these materials, MoV_2S_4 (c and f) had the finest microstructure with an average particle size ca. 1 μm. NiV_2S_4 (b and e) showed some slight signs of particle coarsening, a phenomenon that may be associated with the small fluctuations in value of R_p^{HF} for this material.

3.3. Fuel cell performance and stability

Although symmetrical cells offer a number of advantages, many chemical and electrochemical reactions can be affected by a change of electrode potential, and so it is important to investigate performance of anode materials under non-equilibrium conditions (current flow). Some rate-limiting processes observed in EIS spectra at OCV conditions may significantly speed up, in which case their contributions to overall polarization resistance change. Vanadium-based ternary transition metal sulfide not only had the lowest polarization resistances among the materials described herein, but possessed the higher electronic conductivity (lower resistance) necessary for use as effective anode materials in dynamic electrochemical applications. They were, therefore, selected for subsequent studies in fuel cells having the configuration [H_2S, AV_2S_4–YSZ/YSZ/Pt, air]. Impedance spectra of full cells at 800 °C show the same trend as in the symmetrical set-up, and the cell with MoV_2S_4 anode had the lowest overall polarization resistance (Fig. 4). Only for the case of a cell with MoV_2S_4 anode was the value of the ohmic resistance comparable to that of the polarization one. In the other two cases, the value of cell polarization resistance dominated the overall EIS spectra compared to R_s. Spectra shown in Fig. 4 also include a contribution from cathode impedance. Standard Pt paste cathode was used in all cases. Although all process and application parameters were kept the same, minor fluctuations in cathode performance occurred, but these were sufficiently small to be considered negligible for the present analysis. Fuel cell ohmic resistance was dominated by the contribution from the 0.3-mm thick YSZ electrolyte, and its value varied by no more than 0.2 Ω between cells.

In addition to overall EIS spectra, individual anode and cathode spectra also were measured. The sums of the individual spectra for the two independent half-cells each matched those for the full cells.

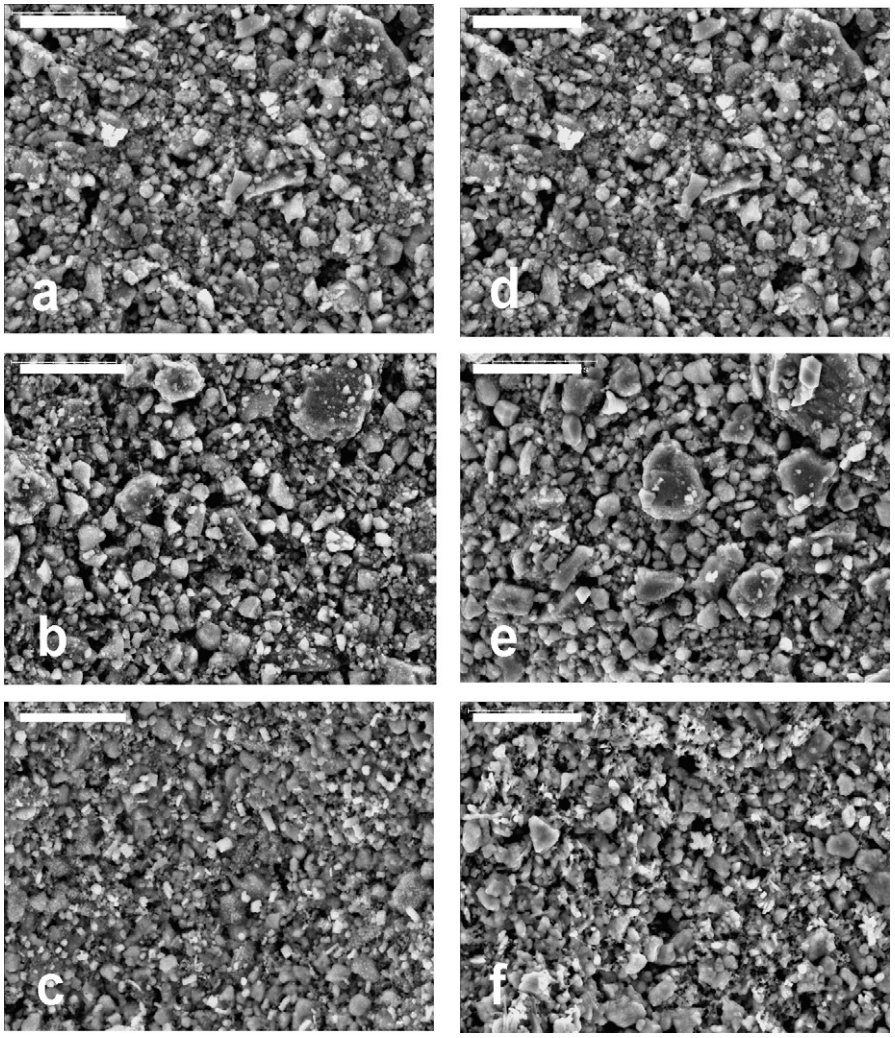

Fig. 3. SEM micrographs of anode materials before test (left) and after test (right). (a, d) CrV_2S_4; (b, e) NiV_2S_4, (c, f) MoV_2S_4; bar scale is 15 μm.

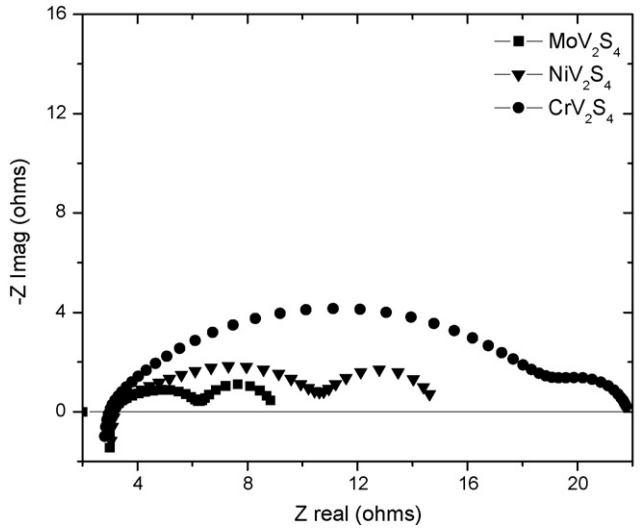

Fig. 4. Fuel cell impedance spectra of vanadium-based anode catalysts at 800 °C.

Consequently, the individual data for each half cell are considered to be reliable. For all cells, each having different anode materials, anodic polarization resistance was the dominating factor in the overall spectra. Another important feature was the presence of a low frequency arc in both overall and anodic EIS spectra, which appeared to be very similar for all anodes regardless of materials and microstructure. Although cathode spectra also contained a low frequency arc, its magnitude was 6–10 times smaller than that for the anodes (ca. 0.3 $\Omega\,cm^2$ vs. ca. 2.6 $\Omega\,cm^2$).

Fig. 5 presents anodic polarization curves for all three V-containing anode materials. It can be seen that MoV_2S_4 had the lowest potential loss compared to those of NiV_2S_4 and CrV_2S_4. Anodic polarization resistance was obtained from the slope of the $I-\eta_a$ curve near $\eta_a = 0$. In theory, the value of R_{pa} obtained using a symmetrical cell, the anodic part of an EIS spectrum using an asymmetric cell, and the slope near OCV of the $I-\eta_a$ curve should all match. In practice, this is difficult to achieve unless there is very strong control of a number of preparation and operation parameters that are difficult to precisely replicate, such as size of the triple-phase boundary, electrode morphology, the presence of impurities and degree of electrode activation [16–18]. Hence a close match normally is considered satisfactory. In our case, a good match was obtained between R_{pa} values obtained from anodic EIS spectra of the asymmetrical cell and slopes of $I-\eta_a$ curve. However, values of anodic polarization resistance obtained on symmetrical cells were almost a factor of two smaller, especially in cases of NiV_2S_4 and CrV_2S_4 anodes. Nevertheless, the general trend of electrochemical activity for H_2S oxidation was identical in all cases $MoV_2S_4 > NiV_2S_4 > CrV_2S_4$. It is at present unknown whether the reduction in anodic polarization resistance for each material was attributable to one of the factors known to give rise to differences between nominally identical samples of a same material [16–18] or due to a systemic factor.

Another important feature shown in Fig. 5 is the trend of slope in $I-\eta_a$ curve, especially for NiV_2S_4 and CrV_2S_4 anodes. This behavior is indicative of change with temperature of the predominant anodic reaction mechanism or of the limiting step of the process. Either of these causes would similarly affect the curvature of the plots. It will be necessary to perform a more detailed parametric study to distinguish between the two possible explanations.

Fuel cell performances of the three cells are presented in Fig. 6. As the structures of the cells were the same except for the anode catalyst, it was expected that only minor changes would be seen in total ohmic resistance and cathode activity between individual cells. Thus the differences in electrochemical character were attributable primarily to differences in performance of anode materials. Fuel cell performances of cells with NiV_2S_4 and CrV_2S_4 catalysts were almost identical (Fig. 6), although EIS of both anodes had significant polarization resistance difference at OCV. Although slopes of *I–V* curves near OCV demonstrated similar trends as in the EIS, the slopes of both curves were almost the same at current densities over 100 mA cm^{-2}, which was consistent with the close values also found for their fuel cell performances. Fuel cell performance of the MoV_2S_4 anode utilizing 100% H_2S anode feed and air at the cathode side remained the highest, with power density ca. 50 mW cm^{-2} at 800 °C.

Several electrochemical tests in two different configurations showed MoV_2S_4 anode materials to have the highest degree of activity for H_2S oxidation at 700–850 °C. Thus it was important to check "ideal" fuel cell performance of this anode in fuel cell mode where ohmic contributions were minimal ($R_s \to 0$). Fig. 7 presents fuel cell test results with ohmic resistance compensation. Power density ca. 275 mW cm^{-2} was achieved at 800 °C and 400 mW cm^{-2} was achieved at 850 °C. By comparison of the IR-compensated curve with the non-compensated *I–V* curve, it is clear that the main loss

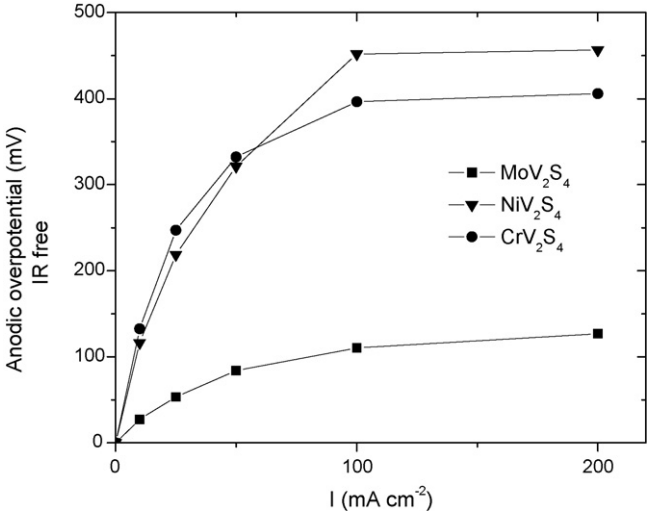

Fig. 5. Anode polarization curves for vanadium-based anodes at 800 °C.

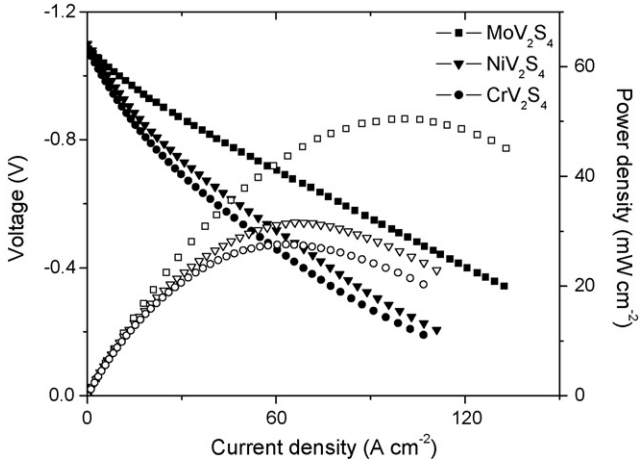

Fig. 6. Fuel cell performance at 800 °C (includes ohmic contribution). Current density–voltage (solid symbols) and current density–power density (open symbols).

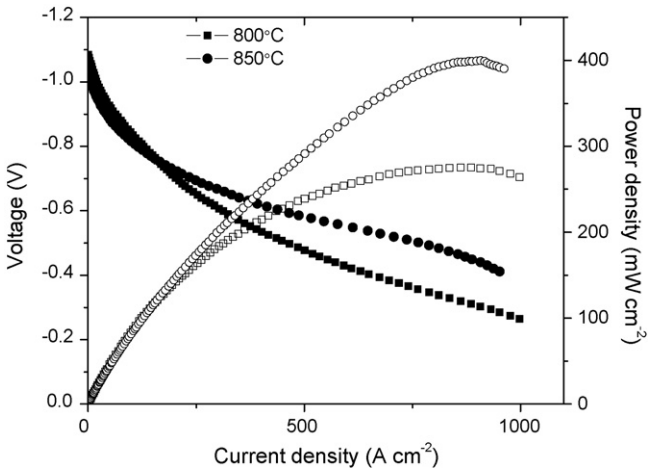

Fig. 7. Maximum attainable fuel cell performance at 800 °C and 850 °C (IR compensated). Current density–voltage (solid symbols) and current density–power density (open symbols).

of potential occurred near low current density values <50 mA cm^{-2}. This region is generally thought to be dominated by activation polarization losses, and is an indicator of activities of fuel cell electrodes.

It was important to confirm chemical stability of materials as well as performance stability of MoV_2S_4-based fuel cells. Powdered MoV_2S_4 sample was exposed to a pure H_2S stream at 850 °C for 10 days. Fig. 8 compares XRD patterns of fresh and after-test samples. The after-test sample had stronger peak intensities, which indicated that the treated sample had even higher crystallinity than the fresh material. There was an increase in a background signal which may indicate presence of a small amount of an amorphous sulfur phase formed from thermal dissociation of H_2S during testing at 850 °C. There were no major peak changes or shifts for the MoV_2S_4 phase, which showed that no significant chemical or phase transformation had taken place during prolonged exposure of the anode material to H_2S at 850 °C. However, for the used sample, two small peaks were seen at $2\theta = 25°$ and 68°, which appeared to have become visible owing to the increased crystallinity of the after-test sample compared with the fresh sample, for which some minor peaks were not well-resolved. Thus small peaks arising from any small amount of impurity also may not have been detectable. In a second stability test, MoV_2S_4-based anodes were tested for electrochemical stability when used in fuel cell mode using the configuration: [H_2S,

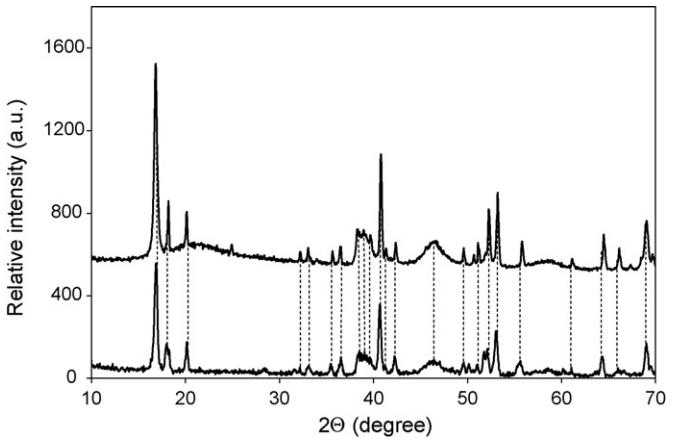

Fig. 8. XRD spectra of MoV_2S_4 powdered samples (bottom–fresh sample and top–after tested in H_2S for 10 days).

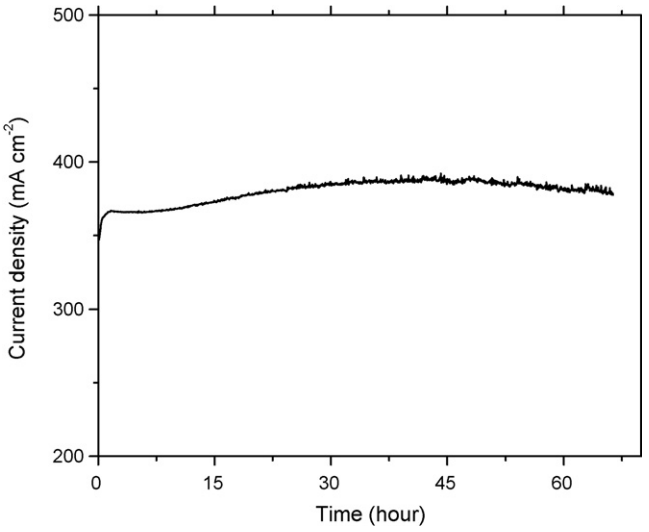

Fig. 9. Fuel cell current density as a function of exposure time to H_2S stream at 850 °C (at constant anodic overpotential of 0.6 V applied across anode-reference electrodes).

MoV_2S_4–YSZ/YSZ/Pt, air] at 850 °C. During these tests a constant overpotential was applied across the anode-reference electrodes' interface and cell current was measured as a function of time. The reference electrode was used to discriminate the anode performance. Fig. 9 shows that there was a stable 370 mA cm^{-2} current over at least 3 days.

There was a build up of sulfur at the exit to the anode chamber during prolonged testing, formed from dissociation of H_2S and/or reaction between H_2S and SO_2. Performances of the stable systems were consistent until experiments were terminated because of impending tube plugging.

4. Conclusions

The ternary transition metal sulfides under investigation in this work are stable and are potential anode materials for H_2S-powered SOFC. The relative activities of these materials for H_2S oxidation are in the order $MoV_2S_4 > NiV_2S_4 > CrV_2S_4 > CuCr_2S_4 > MoS_2 > MoS_2$–$Ni_{3\pm x}S_2 > CoMo_2S_4 > FeCr_2S_4$ within the range 700–850 °C. Vanadium-based sulfides AV_2S_4 possess the highest electronic conductivity.

The IR compensated fuel cell performance using a MoV_2S_4 anode has at least maximum power density 400 mW cm^{-2}. Thus this anode material has high potential for use in highly concentrated H_2S SOFC at 700–850 °C.

EIS and $i - \eta_a$ results show that potential loss was dominated by anodic reactions.

MoV_2S_4 is chemically, structurally and electrochemically stable during prolonged exposure in a pure H_2S stream at 850 °C, as shown by XRD, SEM and fuel cell test results.

Acknowledgements

Financial support from Shell Global Solutions is gratefully acknowledged. We thank Dr. J. Melnik for very helpful discussions.

References

[1] J. Ober, US Geological Survey Minerals Yearbook, Sulfur, US Geological Survey, 2004, pp. 74.1–74.18.
[2] J. Zaman, A. Chakma, Fuel Process. Technol. 41 (1995) 159–198.
[3] N. Pujare, K. Tsai, A. Sammells, J. Electrochem. Soc. 136 (1989) 3662–3678.

[4] A.F. Sammells, J. Patel, J. Osborne, R.L. Cook, Gas Sep. Purif. 6 (3) (1992) 141–147.
[5] B.G. Ong, T.A. Lin, D.M. Mason, Proceedings of the Electrochemical Society Series 12, 1987, 295–306.
[6] D. Weaver, J. Winnick, J. Electrochem. Soc. 134 (1987) 2451–2458.
[7] L. Aguilar, S. Zha, Z. Cheng, J. Winnick, M. Liu, J. Power Sources 135 (2004) 17–24.
[8] C. Yates, J. Winnick, J. Electrochem Soc. 146 (1999) 2841–2844.
[9] M. Liu, P. He, J.L. Luo, A.R. Sanger, K.T. Chuang, J. Power Sources 94 (2001) 20–25.
[10] M. Liu, G. Wei, J. Luo, A.R. Sanger, K.T. Chuang, J. Electrochem. Soc. 150 (2003) A1025–A1029.
[11] G. Wei, J. Luo, A.R. Sanger, K.T. Chuang, J. Electrochem. Soc. 151 (2004) A232–A237.
[12] V. Vorontsov, W. An, J.L. Luo, K.T. Chuang, J. Power Sources 179 (1) (2008) 9–16.
[13] V. Vorontsov, J.L. Luo, K.T. Chuang, US Patent Application, Serial No. 60/950,979 (2007).
[14] A. Wold, Solid State Chemistry: Synthesis, Structure, and Properties of Selected Oxides and Sulfides, Chapman & Hall, New York, 1993 (Chapter 11).
[15] B. Boukamp, Solid State Ionics 20 (1986) 31–44.
[16] M.J. Jorgensen, S. Primdahl, M. Mogensen, Electrochim. Acta 44 (1999) 4195–4201.
[17] M.J. Jorgensen, M. Mogensen, J. Electrochem. Soc. 148 (5) (2001) A433–A442.
[18] S. McIntosh, S. Adler, J. Vohs, R. Gorte, Electrochem. Solid-State Lett. 7 (5) (2004) A111–A114.